Multidetector CT for Evaluation of the Extrapleural Space[1]

Mario G. Santamarina, MD
Ignacio Beddings, MD
Guillermo V. Lermanda Holmgren, MD
Hector Opazo Sanchez, MD
Mariano M. Volpacchio, MD

Abbreviations: EPS = extrapleural space, ETF = endothoracic fascia, IIM = innermost intercostal muscle, MPM = malignant pleural mesothelioma, NSCLC = non–small cell lung cancer

RadioGraphics 2017; 37:1352–1370

https://doi.org/10.1148/rg.2017160180

Content Codes: CH CT OI

[1]From the Department of Radiology, Hospital Naval Almirante Nef, Subida Alessandri S/N, Viña del Mar 2520000, Chile (M.G.S., G.V.L.H.); Departments of Radiology (M.G.S.) and Pathology (H.O.S.), Hospital Dr Eduardo Pereira, Valparaíso, Chile; Department of Radiology, Pontificia Universidad Católica de Chile, Santiago, Chile (I.B.); Department of Pathology, Universidad Andrés Bello, Viña del Mar, Chile (H.O.S.); and Department of Diagnostic Imaging Centro Rossi, Buenos Aires, Argentina (M.M.V.). Recipient of a Magna Cum Laude award for an education exhibit at the 2013 RSNA Annual Meeting. Received July 26, 2016; revision requested January 30, 2017, and received April 3; accepted April 19. For this journal-based SA-CME activity, the authors, editor, and reviewers have disclosed no relevant relationships. **Address correspondence to** M.G.S. (e-mail: *mgsantama@yahoo.com*).

SA-CME LEARNING OBJECTIVES

After completing this journal-based SA-CME activity, participants will be able to:

- Describe the normal anatomy of the EPS.
- List diseases that involve the EPS.
- Recognize the multidetector CT signs that are typical of certain diseases of the EPS and thus facilitate a differential diagnosis.

See www.rsna.org/education/search/RG.

The extrapleural space (EPS) is an anatomic space at the periphery of the chest that can be involved in a number of disease processes. This space lies between the inner surface of the ribs and the parietal pleura and contains adipose tissue, loose connective tissue, lymph nodes, vessels, endothoracic fascia, and the innermost intercostal muscle. It is often overlooked on cross-sectional imaging studies and almost invariably overlooked on conventional radiographic studies. At conventional radiography, the EPS occasionally can be seen when there is extrapleural fat proliferation, which might be confused with pleural thickening or pleural effusion. Knowledge of the normal anatomy of the EPS depicted at computed tomography (CT) and of the relationship of the EPS with parenchymal, pleural, and chest wall processes is key to the detection of extrapleural abnormalities. Disease entities that most commonly affect the EPS include chronic inflammatory disorders, infection, trauma, and neoplasms. Chronic inflammatory conditions and infectious processes of the lungs and pleurae induce adipocyte proliferation adjacent to the inflamed tissue, resulting in increased extrapleural fat. Chest wall trauma with extrapleural hematoma formation causes characteristic CT findings that enable differentiation of the extrapleural hematoma from hemothorax and warrant a different treatment approach. Extrapleural air is commonly seen in patients with pneumomediastinum and should be distinguished from pneumothorax because it requires a different treatment approach. Intrathoracic neoplasms can cause an increase in the attenuation of normal extrapleural fat owing to pleural inflammation, lymphatic obstruction, lymphangitic spread, or direct invasion by tumor. The normal and pathologic appearances of the EPS, as depicted at thoracic CT, and the differential diagnosis of findings in the EPS are reviewed.

Introduction

The extrapleural space (EPS) is an anatomic region between the inner surface of the ribs and the parietal pleura. Although the importance of the EPS as a resection plane is well recognized by surgeons who perform extrapleural pneumonectomies (1), the EPS is not easily visualized radiologically and is frequently overlooked when interpreting thoracic computed tomographic (CT) findings. Nevertheless, the EPS is an important anatomic space from a diagnostic and therapeutic perspective. An understanding of the normal CT appearance of the EPS and the pathologic processes that affect this space helps guide appropriate treatment. In this review, we describe the relevant anatomy of the EPS and review diseases involving the EPS, placing emphasis on imaging findings that aid in rendering the diagnosis and can affect clinical care.

TEACHING POINTS

- At CT, the layers of the EPS more typically manifest as the intercostal stripe, a 1–2-mm-thick linear area of soft-tissue attenuation. The intercostal stripe represents a combination of the visceral pleura, parietal pleura, extrapleural adipose tissue, ETF, and IIM.
- Chronic inflammation of the pleura can result in prolonged focal, mild immune stimulation that induces the proliferation of adipocytes adjacent to the inflamed tissue, with consequent increased extrapleural fat deposition.
- In patients who present with symptoms of pleural effusion, increased attenuation of the EPS fat is a CT finding that suggests that the pleural effusion is an exudate, as this finding is typically absent in patients with transudative effusions.
- The finding of internal displacement of a low-attenuating extrapleural adipose tissue layer is known as the extrapleural fat sign and helps to establish the diagnosis of extrapleural hematoma.
- Lymphatic drainage of the parietal pleurae is complex and varies according to specific anatomic locations, with the pleurae draining into the EPS and local-regional nodes.

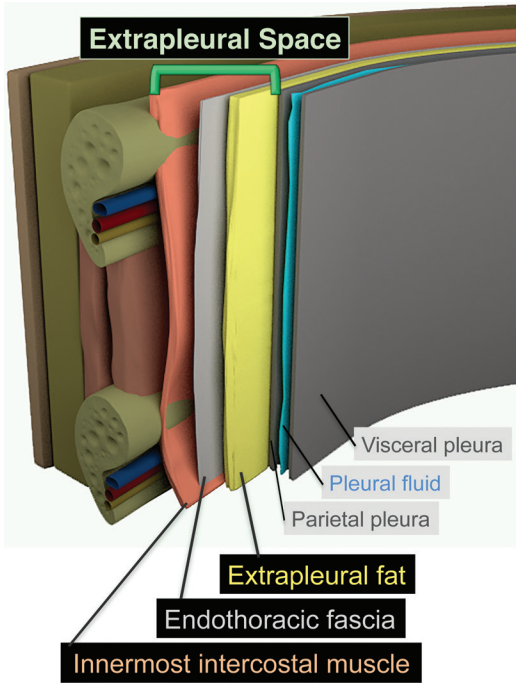

Figure 1. Anatomy of the normal EPS. The EPS lies between the parietal pleura and the inner surface of the ribs and contains adipose tissue, loose connective tissue, lymph nodes, vessels, the ETF, and the IIM.

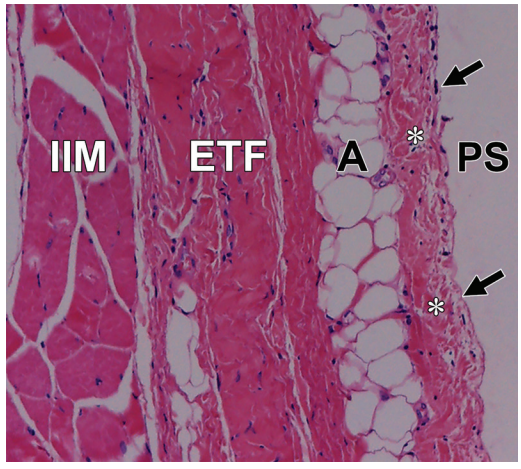

Figure 2. Photomicrograph of a pleural and chest wall biopsy tissue specimen shows the different components of the EPS, including the adipose tissue layer *(A),* ETF, and IIM. The parietal pleura is formed by a single layer of mesothelial cells (arrows) and the fibroelastic layer (*), which includes a basal lamina, submesothelial connective tissue, and a thin superficial elastic layer that is considered to be merged with the rest of the connective tissue. The lymphatic drainage network lies interspersed within the pleural and extrapleural layers. Normal lymph nodes are found mainly in the extrapleural adipose tissue. *PS* = pleural space. (Hematoxylin-eosin stain; original magnification, ×100.)

Anatomy of the EPS

The EPS lies between the outer surface of the parietal pleura and the inner surface of the ribs and diaphragm. It contains adipose tissue, loose connective tissue, lymph nodes, vessels, the endothoracic fascia (ETF), and the innermost intercostal muscle (IIM) (Figs 1, 2). In 1974, Vix (2) provided a comprehensive description of the macroscopic characteristics and distribution of adipose tissue, the main component of the EPS, in a cadaveric study. The adipose tissue in the EPS has variable thickness (average thickness, 250 μm), is located immediately external to the parietal pleura, and separates the pleura from the ETF (3). The ETF is a loose, approximately 250-μm-thick connective tissue layer that covers the inner surface of the IIMs, ribs, costal cartilages, and sternum and blends with the prevertebral fascia posteriorly to form a fibroelastic layer that lines the thoracic cavity (3,4). The IIM, located between the ETF and ribs, extends between the internal surfaces of adjacent ribs in most of the lateral aspect of the chest wall, but it is incomplete in the anterior and posterior aspects of the chest wall. The IIM is replaced anteriorly by the transversus thoracis muscle, which originates from the lower sternum and xiphoid process and extends to the second through sixth costal cartilages, and posteriorly by the subcostal muscles, which originate from the inner surface of a rib and extend to the inner aspect of another rib located one or two intercostal spaces below (4). The intercostal vessels are located externally to the plane of the inner surface of the ribs and as such are considered to be outside of the EPS. However, in the intercostal spaces, the external boundary of the EPS is not visible and appears to fuse with the intercostal space adipose tissue. In our opinion, this explains why some intercostal vessels can sometimes appear to be within an area of extrapleural adipose tissue proliferation.

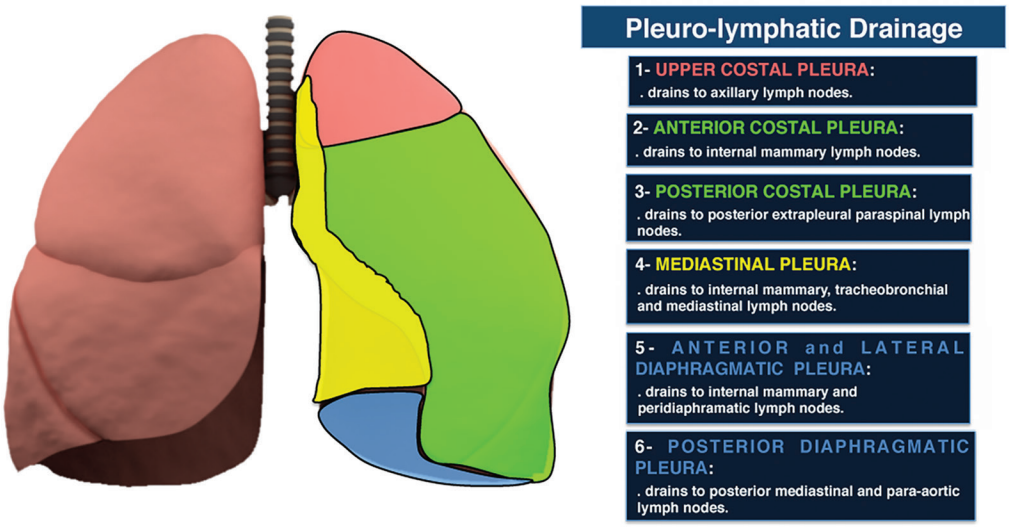

Figure 3. Drawing (left) and corresponding outline (right) illustrate the lymphatic drainage of the parietal pleurae according to disease location. Right: Text is colored to match the corresponding regions on the drawing.

Lymphatic Pathways of the EPS

Knowledge of the lymphatic pathways that drain through the EPS can help the radiologist evaluate the pathways of involvement of different pathologic processes.

The drainage system starts with stomata, which are 0.5–20.0-μm–diameter round or oval discontinuities of the mesothelium that open into the pleural cavity. They are formed by the confluence of mesothelial cells and submesothelial endothelial lymphatic cells and serve as the entrance point for pleural fluid into the lymphatic capillaries of the submesothelium (the connective tissue that surrounds the mesothelium). Stomata demonstrate no resistance to the passage of large molecules; this explains why the protein concentration and colloid osmotic pressure are similar in pleural fluid and lymph at this point (5–8). The diaphragmatic pleura has the highest stoma density; compared with the costal and mediastinal pleurae, it has 80 times more stomata per square centimeter (5,6,8). Below the mesothelial cells, a netlike formation of connective tissue called the cribriform lamina extends and forms the roof of the lymphatic lacunae (7,9). Lacunae are dilated lymphatic capillaries that receive newly formed lymph from the stomata, which is then directed to collector vessels. Lacunae and collector vessels are mainly located within the fat layer of the EPS, and they are connected through a system of transverse vessels.

The pleural lymphatics are equipped with two types of unidirectional valves that allow the entrance of interstitial fluid into the system, simultaneously preventing backflow to the pleural space and permitting the flow of fluid toward only the larger collectors (5,7,8,10).

Respiratory and cardiogenic mechanical forces, which cause tissue distress and internal thoracic pressure variations, help direct the lymph through the lymphatic vessels in one direction (5–7). There is also reabsorption of pleural fluid by way of transcellular transport in the parietal and visceral mesothelia (6,8).

The visceral and parietal pleurae have different lymphatic drainage routes. The visceral pleura drains toward the pulmonary hila through lymphatic vessels in the lobular and interlobular septae (5).

In contrast, the parietal pleura has different zones that drain toward different lymph node groups. This way, the parietal pleural lymphatic drainage is separate from the drainage of the lung and visceral pleura, with most of the structures that form the parietal pleural lymphatic system situated within the connective and adipose tissues that surround the parietal pleural mesothelium (Fig 2) (5–7).

Thus, the patterns of extrapleural lymph node involvement can be predicted according to the location of infection or malignancy in the thorax (11,12). Lymph nodes in the EPS are closely related to the parietal pleural lymphatic system. Lymphatic drainage of the parietal pleurae is complex and varies according to specific anatomic locations, with the pleurae draining into the EPS and local-regional nodes (Fig 3) (5–7).

The mediastinal parietal pleura drains into the internal mammary, tracheobronchial, and mediastinal lymph nodes. The upper costal parietal pleura drains into the axillary lymph nodes (Figs 3, 4). The anterior costal parietal pleura drains into the internal mammary lymph nodes (Figs 3, 5), and the posterior costal parietal pleura drains into the

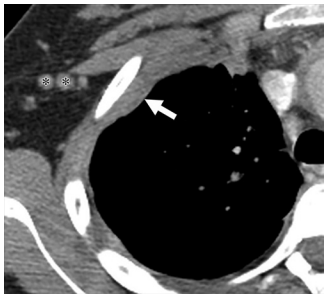

Figure 4. Lymphatic drainage of the upper costal pleura. Axial CT image shows axillary lymph nodes (*) and focal pleural thickening (arrow) secondary to pleural tuberculosis.

Figure 5. Lymphatic drainage of the mediastinal and anterior costal pleurae in a patient with malignant pleural mesothelioma (MPM *[M]*). Axial CT image shows internal mammary (arrow), anterior mediastinal (arrowheads), and hilar (*) adenopathies. *e* = loculated pleural effusion.

Figure 6. Lymphatic drainage of the posterior costal pleura. Axial CT image shows posterior paraspinal extrapleural lymph node metastases (arrows), pleural effusion, diaphragmatic pleural thickening (arrowheads), and costal pleural thickening. Peritoneal carcinomatosis *(Pc)*, lesser curvature gastric carcinoma *(Gca)*, and ascites (*) also are seen. *Sp* = spleen.

posterior paraspinal lymph nodes in the EPS near the heads of the ribs (Figs 3, 6). The anterior and lateral diaphragmatic pleurae drain into the internal mammary and peridiaphragmatic lymph nodes in the EPS (Figs 3, 7). The posterior diaphragmatic pleura drains into the posterior mediastinal lymph nodes adjacent to the esophagus and aorta.

Normal EPS Depicted at CT

The anatomy of the layers that form the chest wall and EPS is complex, mainly because there are many different structures in a very tight space. Thus, spatial resolution is a fundamental aspect of the imaging modality used to study the EPS.

CT is the optimal imaging modality for evaluating the EPS and the pathologic processes that involve this space. The volume data acquired during breath holding can be reconstructed into thin sections that enable soft-tissue window (level, 40 HU; width, 400 HU) evaluation of the EPS with excellent spatial resolution. This permits visualization of the intercostal stripe, which is the manifestation of the normal EPS seen at multidetector CT. Multiplanar (sagittal, coronal, and oblique) reformatting capability and intravenous contrast material administration further enhance the evaluation of pathologic processes that involve the EPS. CT is mainly used to further characterize the abnormalities previously seen at chest radiography or ultrasonography (US) and usually can be used to more precisely determine whether a peripheral abnormality is parenchymal, pleural, or extrapleural in origin.

Chest radiography can be useful for evaluating pleural or extrapleural abnormalities that are large enough to be detected with the technique. However, it may not provide the spatial resolution that is necessary to localize a lesion to the pleura, EPS, or chest wall. The normal pleura can be seen where the visceral pleura folds, invaginating the lung to form the fissures, and where the lungs come in contact to form junction lines. However, EPS structures cannot be precisely depicted with chest radiography alone.

US also can be used to assess the pleura and chest wall structures, with the intercostal

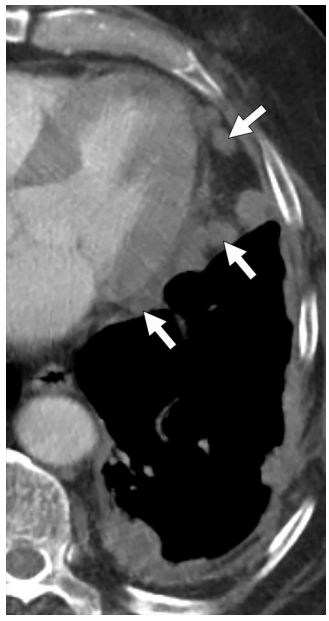

Figure 7. Lymphatic drainage of the anterior diaphragmatic pleura. Axial CT image shows anterior paracardiac and diaphragmatic lymph node metastases (arrows). Note the lobulated pleural thickening due to MPM.

Figure 8. Normal CT appearance of the EPS. Axial CT image of the right side of the chest shows the intercostal stripe (large arrows) as a 1–2-mm-thick linear area of soft tissue in the anterolateral and posterolateral intercostal spaces, at the point of contact between the lung and chest wall. This stripe represents a combination of the visceral pleura, parietal pleura, extrapleural adipose tissue, ETF, and IIM, which is the main component. The intercostal stripe is incomplete in the anterior parasternal and posterior paravertebral areas of the chest wall. The paravertebral line (small arrow) in the posteromedial aspect of the chest wall represents the ETF and the parietal and visceral pleurae. The transversus thoracis muscle (arrowhead) is seen along the parasternal region of the chest wall as a stripe of soft-tissue attenuation in the same plane as the IIM.

space used as a sonographic window. The pleural surface forms a reflective band immediately deep to the chest wall structures. This reflective band results from high-amplitude echoes at the lung-pleura interface, but it also encompasses the ETF, parietal pleura, and visceral pleura. US enables recognition of the dermoepidermic plane, subcutaneous tissue, intercostal muscles, ribs, pleural band, and lungs. It can also depict EPS abnormalities such as masses and fluid collections. However, the narrow field of view and lack of dynamic contrast enhancement information limit US evaluation of the pathologic processes.

Magnetic resonance (MR) imaging also can be used to evaluate chest wall and extrapleural abnormalities, with respiratory compensation and cardiac gating used when necessary. However, neither the normal pleural surfaces, fissures, and junctional lines nor the separate layers that form the EPS are usually seen at MR imaging owing to the limited spatial resolution of the technique and the susceptibility effects that result from the neighboring air-containing lung interface. On the other hand, the excellent contrast resolution combined with multiplanar imaging capability, contrast material–enhanced sequences, and dynamic sequences of MR imaging are ideal for tumor characterization and evaluation of tumor extension into the EPS from adjacent structures such as the lungs, or tumor extension from the EPS into neighboring tissues (13).

The layers of the EPS are not distinguishable as separate structures on CT images (3). At CT, the layers of the EPS more typically manifest as the intercostal stripe, a 1–2-mm-thick linear area of soft-tissue attenuation. The intercostal stripe represents a combination of the visceral pleura, parietal pleura, extrapleural adipose tissue, ETF, and IIM, with the IIM being its main component (13,14). The intercostal stripe is seen in the anterolateral and posterolateral aspects of the intercostal spaces, at the point of contact between the lung and chest wall (Fig 8) (13). The intercostal stripe is usually not visible in the anterior parasternal and posterior paravertebral regions of the chest owing to the absence of the IIM in these locations. However, the para-

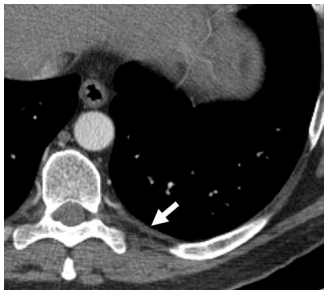

Figure 9. Normal CT appearance of the EPS. Axial CT image of the lower left region of the chest shows the subcostal muscle (arrow) in a paravertebral location. The subcostal muscle originates from the inner surface of the ribs and extends to the inner aspect of another rib located one or two intercostal spaces below.

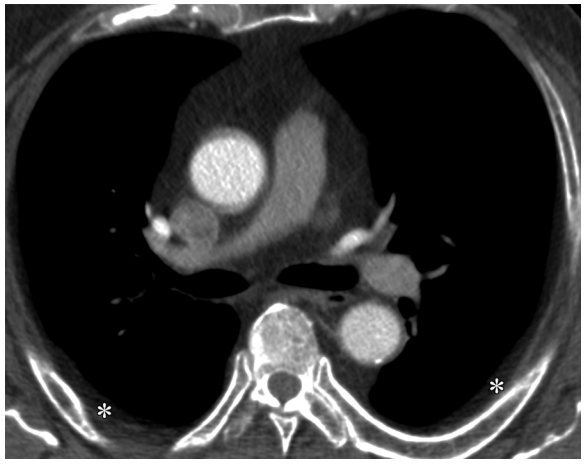

Figure 10. Nonpathologic extrapleural adipose tissue in an obese patient. Axial CT image shows increased adipose deposits (*) in the EPS.

vertebral line, representing the visceral pleura, parietal pleura, and ETF, without the IIM, occasionally can be seen in the posteromedial aspect of the chest, occupying the same plane as the intercostal stripe (Fig 8). The transversus thoracis (Fig 8) and subcostal (Fig 9) muscles, located in the parasternal and paravertebral aspects of the chest, respectively, can manifest as a stripe in the same plane as the intercostal stripe. Intercostal vessels can be distinguished from intercostal muscles on the basis of their tubular shape, which can be better depicted on reformatted sagittal or coronal images. They can also be distinguished from the intercostal muscles by their sometimes tortuous path and their location within the costal groove; however, variability in their location has been described. In addition, intercostal vessels show enhancement similar to that of the larger thoracic vessels (15).

In obese persons, individuals involved in chronic glucocorticoid use, and some healthy individuals, an increase in adipose tissue can be seen in the EPS, internal to the plane of the IIM. In these cases, adipose tissue can be seen on CT images as bilateral, symmetric focal collections of extrapleural fat up to several millimeters thick in the midlateral region of the thorax, immediately internal to the ribs, and in the intercostal spaces in the region between the fourth and eighth ribs (Fig 10) (2,3). This finding can also be seen in the same locations on chest radiographs.

The Abnormal EPS

Chronic inflammation, infection, trauma, and neoplasms can involve the EPS. In addition, the EPS can become involved with a variety of infiltrative processes. The causes, manifestations, and multidetector CT findings of these pathologic processes in the EPS are described and listed in the following sections and in the Table.

Inflammation

Chronic inflammation of the pleura can result in prolonged focal, mild immune stimulation that induces the proliferation of adipocytes adjacent to the inflamed tissue, with consequent increased extrapleural fat deposition. This extrapleural fat proliferation is the result of paracrine interactions between adipose tissue and lymphoid tissue, which also improve local immune function (16,17).

Thickening of the extrapleural fat, as detected on CT images, is indicative of a chronic benign cause of the adjacent pleural thickening. However, this feature may also be present—albeit less commonly—with malignancy (18,19). This extrapleural fat thickening can be seen with hemothorax, which can result in pleural fibrosis, pleural calcification, and fat proliferation in the EPS (Fig 11) (20). Blood clots in the pleural space occur frequently and may be difficult to drain. Although there is little evidence suggesting that blood alone can cause a fibrothorax, in the setting of mesothelial cell and pleural basement membrane injury, the fibrin meshwork from coagulated blood may serve as a provisional matrix for connective tissue formation in the pleural space. Thus, the risk of fibrothorax would depend on the amount of undrained blood and the degree of pleural injury (20).

Rounded atelectasis and asbestos-related pleural disease are frequently associated with pleural fibrosis, which can be related to an increase in EPS fat that results from chronic inflammation (21,22). Rounded atelectasis is a benign inflammatory process that typically manifests at CT as a masslike opacity with an indistinct central margin, converging vessels, and bronchi that are tractioned by the central opacity, forming the "comet tail"

Multidetector CT Findings of EPS Disease Processes

CT Finding and Causes	Related Disease or Condition
Fatty expansion of the EPS	
Pleural inflammation	Pleural exudates
	Empyema
	Asbestos-related pleural disease
Neoplasm	Metastatic NSCLC
	MPM
Mimicking condition	Posterior diaphragmatic defect
	Lipoma
Systemic condition*	Obesity
	Chronic glucocorticoid use
Soft-tissue stranding of the extrapleural fat	
Pleural inflammation	Empyema
Neoplasm	Metastatic NSCLC
	MPM
Abnormal attenuation in the EPS	
Blood (extrapleural hematoma)	Trauma
	Iatrogenic injury
	Anticoagulant therapy
	Coagulopathy
Air (extrapleural air collections)	Barotrauma
	Tracheobronchial tree disruption
	Esophageal disruption
	Extension of air from other spaces (eg, neck, retroperitoneum)
Soft-tissue expansion of the EPS	
Nonneoplastic	Inflammatory process
	Extramedullary hematopoiesis
	Amyloidosis
	Thoracic splenosis
	Extrapleural plombage
Neoplastic	Chest wall neoplasms
	Lung cancer
	Pleural malignancies
	Lymphoproliferative disorders
	Neurogenic tumors

Note.—NSCLC = non–small cell lung cancer.
*Systemic conditions can also occur in healthy individuals.

sign. Rounded atelectasis is associated with pleural effusion and/or thickening. Although extrapleural fat thickening is not a constant finding of rounded atelectasis, its presence is an indicator of chronic inflammation, which supports the diagnosis of rounded atelectasis (Fig 12) (22). Asbestos exposure is the most common etiologic factor of rounded atelectasis, accounting for 29%–86% of cases (22). However, exudative pleural effusions and less commonly transudative pleural effusions also can result in the development of rounded atelectasis, in the absence of asbestos or other mineral dust exposure. In fact, pleuritis is the second leading cause of rounded atelectasis, accounting for approximately 14%–64% of cases (22–24).

Asbestos exposure can also cause an increase in adipose tissue in the EPS owing to chronic inflammation. Increased EPS adipose tissue related to asbestos exposure can also be seen in association with the formation of parietal pleural plaques, which develop 20–30 years after the onset of the exposure to asbestos (Fig 13) (23,25). Increased attenuation of the extrapleural fat at CT can occur with pleural exudates, such as those seen in patients with reactive mesothelial hyperplasia due to asbestos exposure and those with rheumatoid arthritis (26,27). Pleural effusion is the most common intrathoracic manifestation of rheumatoid arthritis, can precede the first signs of joint disease, and is asymptomatic in the majority of patients (28). In patients who present with symptoms of pleural effusion, increased attenuation of the EPS fat is a CT finding that suggests that the pleural effusion is an exudate, as this find-

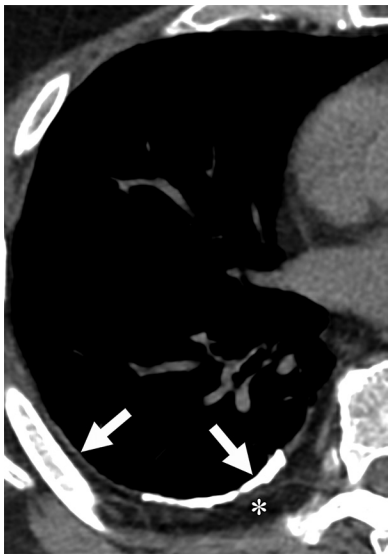

Figure 11. Pleural fibrosis secondary to prior hemothorax. Axial CT image shows pleural plaques with associated thick coarse calcifications (arrows). Note the thickened extrapleural adipose tissue (*).

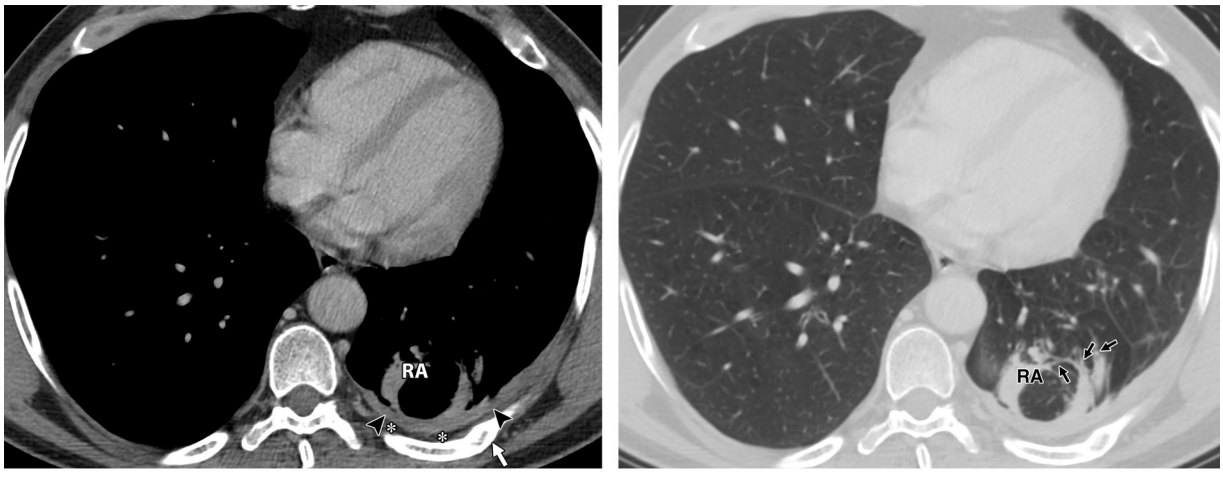

a. **b.**

Figure 12. Rounded atelectasis *(RA)* with associated pleural thickening and extrapleural adipose tissue thickening. **(a)** Axial chest CT image obtained in the mediastinal window through the lower region of the chest shows rounded atelectasis, increased extrapleural adipose tissue (*), and pleural thickening (arrowheads). **(b)** Axial chest CT image obtained in the lung window through the same region shows a loss of volume of the left lower lobe and architectural distortion of the lung that surrounds the rounded atelectasis. This distortion results in the classic comet tail sign, which is caused by the traction of vessels and bronchi (arrows) that surround a masslike area of rounded atelectasis. The bronchovascular bundles appear to be pulled by the mass and resemble a comet tail. A rib fracture (arrow in **a**), which caused a hemothorax that resulted in the depicted pleural changes, has healed.

ing is typically absent in patients with transudative effusions (19). Although to our knowledge, there are no study data that establish a quantitative way of determining increased extrapleural fat density, a qualitative assessment can be performed by comparing the extrapleural fat density of the affected side either with that of the contralateral side or with the subcutaneous adipose tissue.

Infection

Acute infections of the lung and pleura can result in increased thickness of the EPS fat. Extrapleural fat thickness greater than 3 mm at CT has been reported to occur in up to 60% of patients who have parapneumonic effusion or empyema in association with parietal pleural thickening (29,30). This increase in adipose tissue in the EPS is typically not seen during the acute (exudative) phase; rather, it typically occurs during the subacute (fibrinopurulent) phase of parapneumonic effusion or empyema (Fig 14) and in the organizing phase, which is characterized by fibroblast proliferation and chronic inflammation. In patients with empyema, infiltration of the EPS by inflammatory cells, lymphatic distension, and granulation tissue can result in increased attenuation and expansion of the extrapleural fat (Figs 15, 16) (19,29,30). If the infection is not adequately treated, the pleura may calcify and progress to form a calcified rind of pleura that entraps the lung; this condition is called a fibrothorax

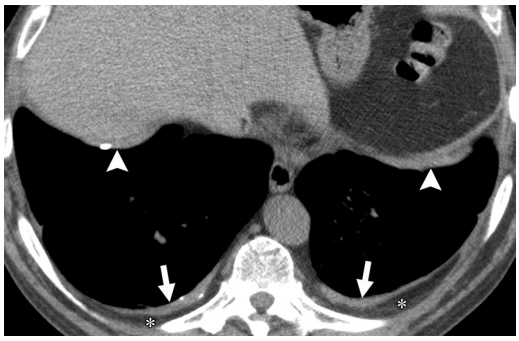

Figure 13. Extrapleural adipose tissue thickening associated with pleural plaques. Axial targeted reconstruction CT image of the posterior region of the chest shows increased extrapleural adipose tissue (*) adjacent to pleural plaques in the posterolateral parietal pleural surfaces (arrows) and dome of the diaphragm (arrowheads). The plaques are secondary to asbestos exposure. The finding of increased extrapleural adipose tissue is useful for determining the chronicity and benign cause of the pleural abnormality.

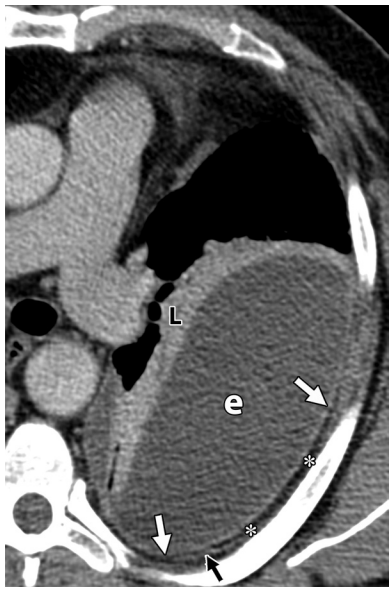

Figure 14. Fibrinopurulent phase of empyema and increased extrapleural adipose tissue. Axial targeted reconstruction CT image of the left hemithorax shows a loculated left pleural effusion *(e)* exerting a mass effect on the adjacent lung *(L),* diffusely thickened and enhancing parietal pleura (white arrows), and an increase in extrapleural adipose tissue (*). Also note the intercostal vein (black arrow).

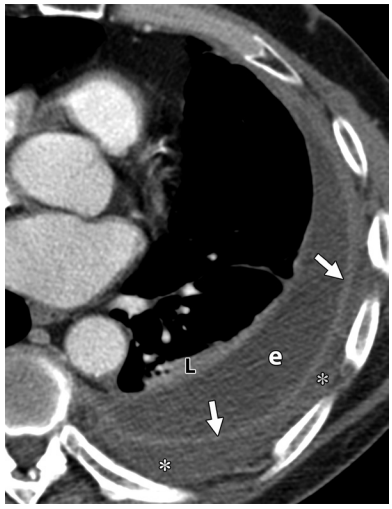

Figure 15. Empyema and increased attenuation of the adipose tissue in the EPS. Axial CT image of the left side of the chest shows increased attenuation and thickness of the EPS (*). Note the thickening and enhancement of the visceral and parietal pleurae (arrows), pleural effusion *(e),* and atelectasis in the adjacent lung *(L).*

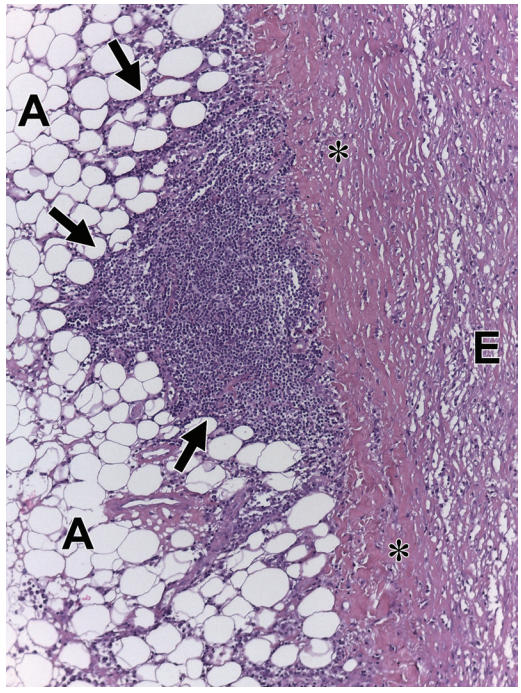

Figure 16. Pleural empyema. Low-power photomicrograph of a pleural and chest wall biopsy tissue specimen shows multiple foci of inflammatory mononuclear cells (arrows) that have infiltrated the extrapleural adipose tissue layer *(A).* The fibroelastic layer (*) and superficial fibrinous exudate *(E)* are seen. (Hematoxylin-eosin stain; original magnification, ×100.)

(Fig 17). When a fibrothorax is formed, contraction of the involved hemithorax and simultaneous extrapleural fat proliferation occur and together limit adequate expansion of the underlying lung (Fig 18). The increased extrapleural fat occupies the space left by the nonexpanded lung, and this increase in adipose tissue could be explained, at least in part, by chronic inflammation that induces local fat proliferation.

Chronic infection of the pleural space, as seen in some patients with tuberculous pleuritis, may result in further complications such as bronchopleural fistula formation and empyema necessitatis. Empyema necessitatis, the spontaneous extension of purulent pleural fluid into the EPS and soft tissues of the chest wall, is most commonly seen as a complication of *Mycobacterium tuberculosis* infection, although *Actinomyces* and *Nocardia* infections can cause similar findings (31,32). The CT findings of infectious process extension into the chest wall include thickening and increased attenuation

Figure 17. Organizing phase of tuberculosis-induced empyema. Axial CT image through the right hemithorax shows dense thick calcifications of the pleura (arrow) and increased extrapleural fat (*).

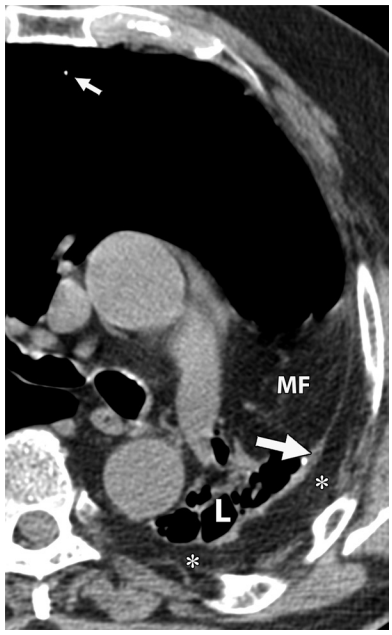

Figure 18. Extensive lung destruction and residual tuberculosis-induced changes. Axial CT image through the left hemithorax shows thickening and calcification of the pleura (large arrow), marked proliferation of the extrapleural fat (*), and cicatricial atelectasis with traction bronchiectasis in the left lung *(L)*. The contralateral lung is hyperinflated, with an isolated calcified granuloma (small arrow). A prominent mediastinal shift is ipsilateral to the cicatricial changes. *MF* = mediastinal fat.

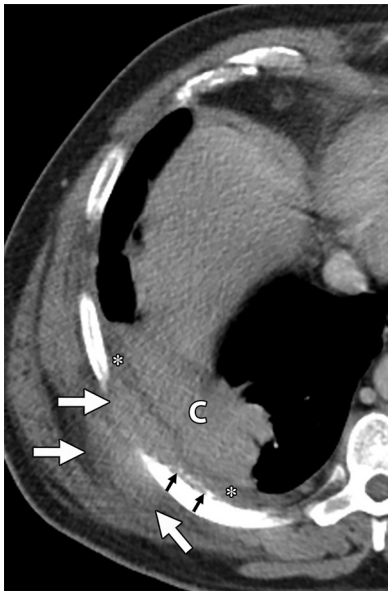

Figure 19. Pulmonary actinomycosis complicated by empyema necessitatis. Axial CT image of the right side of the chest shows right lower lobe consolidation *(C)* and increased thickness and attenuation of the EPS (*). Note the poorly marginated extension of infection into the chest wall (white arrows) and the periosteal reaction (black arrows) in the inner margin of the adjacent rib.

of the extrapleural fat and purulent chest wall fluid collections. In patients with actinomycosis, sinus tracts, fistulas, periosteal reaction, and bone destruction are additional findings (Fig 19) (33).

Empyema necessitatis can be further complicated by rib osteomyelitis (Fig 19) (34,35). Treatment varies according to the clinical setting and the response to initial treatment. Surgical resection of the affected bone tissue followed by antibiotic treatment has been advocated by some authors and in some case reports (34,36,37). This treatment protocol enables confirmation of the diagnosis for patients with negative exudate cultures (36,37). Others (38,39) have reported successful treatment with antibiotic therapy only. Careful identification and evaluation of the intercostal stripe and extrapleural fat can be useful for diagnosing early or limited extension of infection into the adjacent soft tissues of the chest. Radiologists and clinicians should be able to identify these findings before more layers of the chest wall or bone become involved.

Trauma

Chest wall trauma can result in bleeding into the EPS. An extrapleural hematoma develops when an intact parietal pleura prevents blood from draining into the pleural space (40). Blunt chest wall trauma, especially when it is associated with rib fractures, which can injure adjacent vessels, is the most common cause of extrapleural hematoma formation. In this case, the source of the bleeding is usually injured intercostal or internal mammary vessels (41). An extrapleural hematoma can also arise from aortic, great vessel, or mediastinal vascular injury or directly from bleeding of a fractured vertebra or rib (40,41). Penetrating injury, including iatrogenic injury to intercostal vessels (secondary to pleural and chest wall interventional procedures), also can cause an

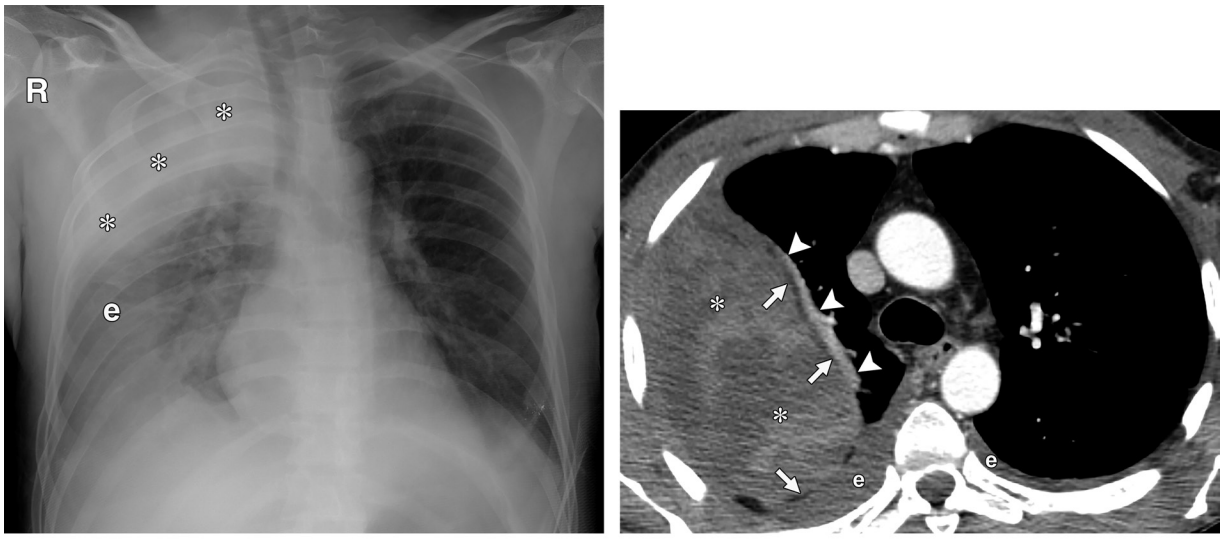

a. b.

Figure 20. Extrapleural hematoma due to vascular injury to the subclavian vessels after attempted right subclavian venous catheterization. **(a)** Frontal chest radiograph obtained after the installation of a central venous catheter shows an apical opacity (*) that was not present on previously obtained images, and associated pleural effusion *(e)*. This finding and context must raise suspicion for subclavian vessel injury. **(b)** Axial cropped CT image findings confirm the presence of a large extrapleural hematoma (*) in the upper third of the right hemithorax. The hematoma is displacing the extrapleural fat (arrows). Associated pleural effusion *(e)* and compressive atelectasis (arrowheads) of the superior right lobe also are seen.

extrapleural hematoma when the parietal pleura is not breached (Fig 20). Spontaneous hematomas can occur in patients with coagulopathy and in cases of connective tissue disease (42). Early diagnosis of extrapleural hematoma is important because bleeding can be rapid and cause respiratory or circulatory compromise (41–43). Furthermore, with more than 50% of extrapleural hematomas, there is an associated hemothorax, and together these bleeding processes account for an even larger blood extravasation (41).

An extrapleural hematoma manifests radiographically as a localized pleura-based extrapulmonary mass with a sharp inner margin and tapered obtuse edges. The absence of an obliterated costophrenic angle can aid in localizing this abnormality in the EPS (41). CT findings include a focal fluid collection, with high attenuation values due to the presence of coagulated blood products (ie, blood attenuation) and sometimes fluid-fluid levels with higher attenuation in the more dependent portions of the hematoma. This fluid collection causes inward displacement of the extrapleural fat. The finding of internal displacement of a low-attenuating extrapleural adipose tissue layer is known as the extrapleural fat sign and helps to establish the diagnosis of extrapleural hematoma in the appropriate clinical setting (40,44). The convex-inward contour of the hematoma and displaced extrapleural fat suggest that the hematoma probably has an arterial origin (Fig 21) (40,44). Conversely, when the displaced extrapleural adipose tissue is only slightly convex or linear, the extrapleural hematoma probably has a venous origin and, thus, no surgical management is required (Fig 22).

Most extrapleural hematomas are treated with close observation or needle aspiration. However, surgical management may be required in some cases if ventilatory or circulatory disturbances occur—especially with expanding extrapleural hematomas such as those in patients with coagulopathy. Given the location of the collection, a typical thoracostomy tube placed in the pleural space will not drain the extrapleural blood, and this is an unnecessary invasive procedure in patients who have an extrapleural blood collection without hemothorax. Thus, accurate characterizaton of a collection as either pleural or extrapleural is important for guiding management (41). In addition to the origin of the bleeding, the size of the hematoma is an important factor in determining treatment, with observation being an option when an extrapleural hematoma with convex displacement of extrapleural adipose tissue is small (40). However, because small convex extrapleural hematomas secondary to arterial bleeding can enlarge rapidly, close clinical observation is recommended (40,44). Large extrapleural hematomas may pose difficulties for surgeons at thoracotomy in terms of identifying the origin of the bleeding. Multidetector CT angiography is a time-efficient method for directing and planning therapy for patients with acute bleeding (45). Thoracic arterial angiography is a diagnostic and therapeutic option, although it involves some risk

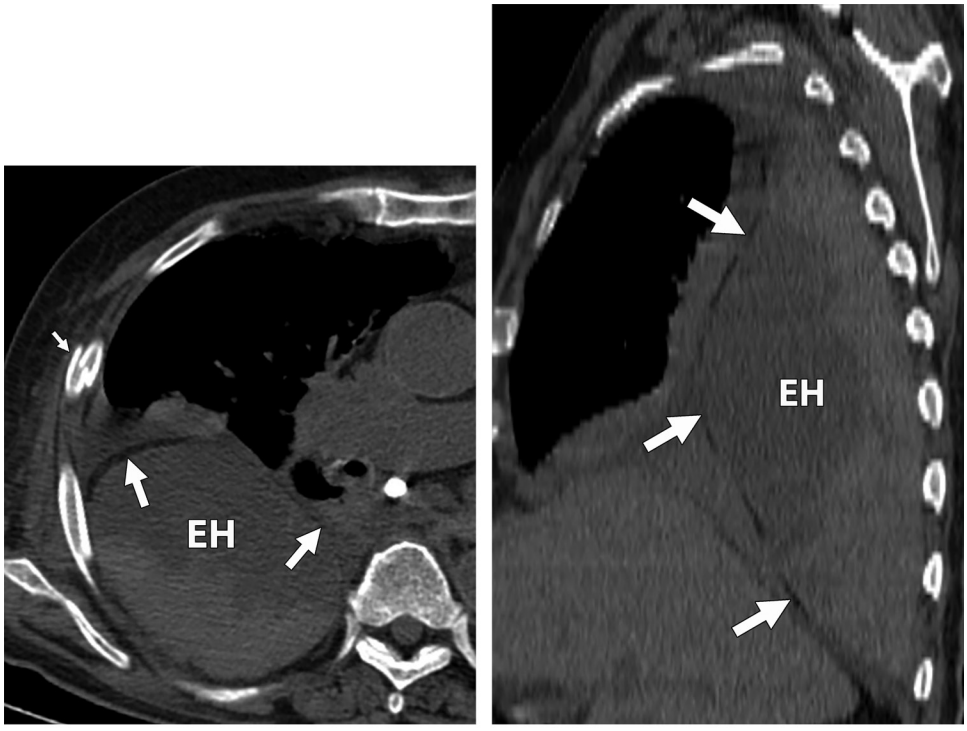

a. **b.**

Figure 21. Extrapleural hematoma secondary to rib fracture. Axial **(a)** and sagittal reconstructed **(b)** CT images of the right side of the chest show an extrapleural hematoma *(EH)* that displaces the extrapleural fat (large arrows) anteriorly and medially, forming the extrapleural fat sign. Extrapleural hematomas are usually associated with rib fractures (small arrow in **a**), as in this case. Note the increased attenuation of the hematoma posteriorly; this is a manifestation of clot formation and is consistent with the presence of subacute hemorrhage. The convex configuration of the displaced EPS adipose tissue denotes an arterial origin of the bleeding, and the large size of the hematoma necessitated surgical management. Extrapleural hematomas are usually associated with rib fractures in patients with blunt trauma.

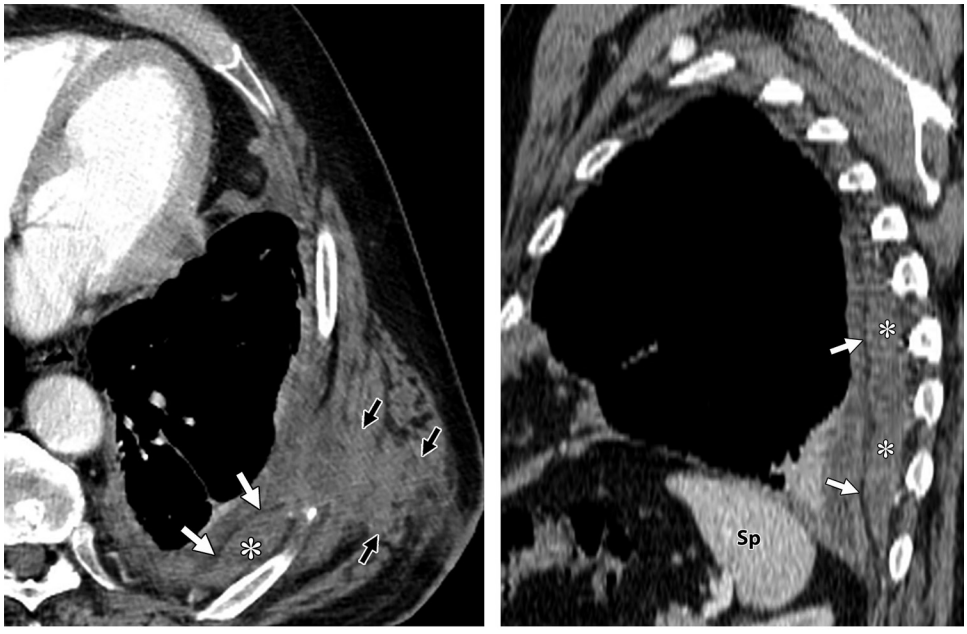

a. **b.**

Figure 22. Extrapleural hematoma secondary to pleural biopsy to diagnose MPM. Axial **(a)** and sagittal reconstructed **(b)** CT images of the left side of the chest show an extrapleural hematoma (*) with linear (superiorly) and slightly convex (inferiorly) displacement of the extrapleural fat (white arrows), suggesting a venous origin of the bleeding. The hematoma resolved spontaneously with conservative management. Postbiopsy changes are seen in the posterolateral aspect of the chest, with increased attenuation of the subcutaneous adipose tissue, irregular laminar blood collections, and lost definition of the margins of the serratus posterior inferior and latissimus dorsi muscles (black arrows in **a**). *Sp* = spleen.

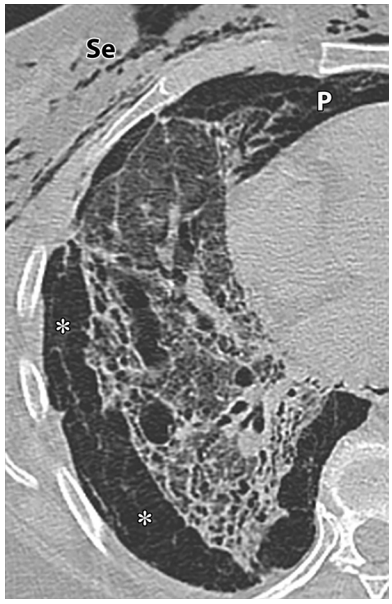

Figure 23. EPS air collection mimicking pneumothorax in a patient with idiopathic pulmonary fibrosis and sudden worsening of dyspnea. Axial CT image of the right side of the chest shows air (*) surrounding the lung and in continuity with pneumomediastinum *(P)*. Weblike linear septa are present in the extrapleural air collection. *Se* = subcutaneous emphysema.

Figure 24. NSCLC and increased attenuation of adipose tissue in the EPS. Axial coned-down CT image of the right side of the chest shows a mass *(M)* invading the adjacent vertebral body. There is increased attenuation of the extrapleural adipose tissue (*) due to extrapleural tumoral involvement. Note the pleural thickening (arrowheads) and associated pleural effusion *(e)*. *D* = diaphragm.

of embolic material being accidentally introduced into the anterior spinal artery (41).

Air within the EPS caused by the extrapleural extension of pneumomediastinum is mainly associated with barotrauma, but it occasionally results from a disruption of the tracheobronchial tree or esophagus. Similarly, extrathoracic air extending into the mediastinum from the neck, chest wall, peritoneal cavity, or retroperitoneum can lead to air in the EPS (46,47). Although air collections in the EPS can mimic pneumothorax, the presence of weblike linear opacities within the air collection on a chest radiograph or CT image can be useful for differentiating an extrapleural air collection from pneumothorax or the extrapleural air sometimes seen in an apparently loculated location (Fig 23) (48). An additional manifestation of an EPS air collection is a focal spherical air collection between the parietal pleura and diaphragm in an infant with pneumomediastinum, a condition known as the extrapleural air sign (49). As with an extrapleural hematoma, with EPS air, accurate localization of the air collection is fundamental for guiding management, because misdiagnosing extrapleural air as pneumothorax will lead to the unnecessary placement of a thoracostomy tube, and most extrapleural air collections with associated pneumomediastinum are treated with close observation. In cases of tracheobronchial tree or esophageal lesions, treatment of these underlying causes will lead to resolution of the extrapleural air collection.

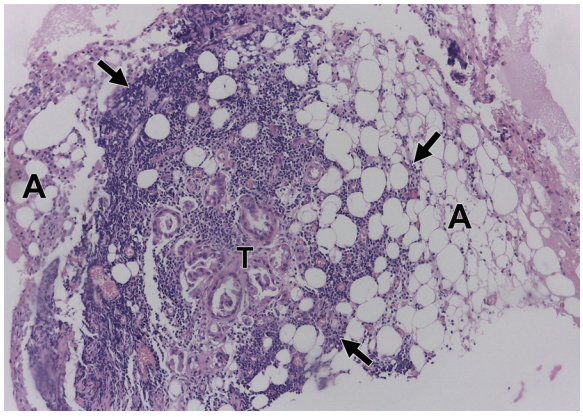

Figure 25. Metastatic adenocarcinoma in extrapleural adipose tissue. Low-power photomicrograph of a pleural and chest wall biopsy tissue specimen shows a focus of invasive adenocarcinoma *(T)* and reactive inflammatory infiltrates (arrows) in the adipose tissue layer *(A)* of the EPS. (Hematoxylin-eosin stain; original magnification, ×100.)

Neoplasms

An increase in EPS adipose tissue thickness and attenuation can be seen in patients with primary intrathoracic peripheral malignancies—mainly NSCLC and MPM (15,50). The increased at-

Figure 26. NSCLC and invasion of the EPS. Axial cropped CT image of the lower region of the chest shows extension (arrow) of a right lower lobe mass *(M)* into the extrapleural fat (*). Note the contralateral side, which lacks the increased extrapleural fat thickness and attenuation.

tenuation can be due to pleural inflammation, lymphatic obstruction, lymphangitic spread, or direct tumor invasion (Figs 24, 25) (19,45).

This increase in attenuation of the extrapleural fat is a CT finding that suggests localized invasion of the parietal pleura and chest wall—an important finding in patients with NSCLC and MPM who are being evaluated for possible resection (12). Chest wall involvement occurs in fewer than 8% of patients with newly diagnosed NSCLC (51).

A primary objective of preoperative staging in patients who present with symptoms of peripheral NSCLC that abuts the pleura is to determine whether chest wall resection is required (52). Invasion of the EPS by a primary NSCLC tumor of any size is categorized as stage T3 disease. In the absence of nodal or distant metastatic disease in a surgical candidate, en-bloc resection—that is, removal of the lung parenchyma in continuity with a portion of the adjacent parietal pleura and chest wall—is considered the treatment of choice (52,53). The most specific CT criterion for detecting chest wall invasion is rib destruction or visible tumor extending into the chest wall; however, these findings are absent in most patients with chest wall invasion. Obliteration of the extrapleural fat plane (Fig 26) is reported to have the highest accuracy for detection of chest wall invasion by a peripheral lung cancer, with a sensitivity of 85% and a specificity of 87% (54). Other CT criteria reported to have accuracy for detection of chest wall invasion by a peripheral lung cancer are length of the area of tumor-pleura contact, ratio of tumor-pleura area length to tumor diameter, a mass involving the chest wall, pleural indentation, and tumor attenuation (53–55). Although respiratory dynamic MR imaging has been proposed as an imaging modality complementary to CT for depiction of chest wall invasion (100% sensitivity, 83% specificity), it is not widely used in this setting (56). Transthoracic US can be used to adequately assess chest wall invasion when CT results are inconclusive, and it is less costly compared with respiratory dynamic MR imaging. It allows dynamic real-time evaluation of the relationship between the mass and the chest wall and can depict movement of the mass in relation to the chest wall during respiration, or the so-called "sliding" sign. This sign has a sensitivity and specificity of 88.9% and 100%, respectively, for predicting the presence of pleural adhesions and an accuracy of 95.6% for detecting chest wall infiltration by NSCLC and lung infiltration by chest wall tumors (57).

MPM, the most common primary pleural malignancy, has a propensity for local invasion, and extension into the chest wall is common. As with the diagnosis of invasion by NSCLC, the diagnosis of chest wall invasion by MPM is important for tumor staging and can lead to a change in treatment in patients who are being evaluated for possible surgery (58–61). A solitary focal region of tumor extending directly into the EPS or chest wall is categorized as stage T3 disease and often occurs at a site of previous biopsy or chest tube insertion owing to tumor extending through previously created tracts (60). The resection protocol for MPM is similar to that for NSCLC in that a single focus of tumor directly invading the chest wall is removed en-bloc with the entire tumor. This is in contrast to the management protocol for multifocal or locally advanced tumor, which is classified as stage T4 disease and is technically nonresectable because it diffusely invades the chest wall musculature (60). At the time of diagnosis, only a minority of patients with MPM are candidates for surgery. These patients have markedly better outcomes when their treatment involves the use of a multimodality approach rather than surgery alone; this finding has been confirmed in retrospective and prospective studies (62). Currently, two main surgical techniques are performed to treat patients with mesothelioma. One technique is extrapleural pneumonectomy (EPP), which involves en-bloc resection of the lung, parietal and visceral pleurae, diaphragm, and pericardium, which have a resection margin through the EPS. The other technique is pleurectomy-decortication, which, as compared with EPP, enables the surgeon to spare the lung. The high risk associated with EPP without a clear demonstration of survival benefits has led many clinicians to advocate against using this technique (63).

Intrathoracic lymphoma has been reported to involve the EPS as a site of recurrent disease in

the chest and in up to 4% of patients with symptoms of mediastinal and/or pulmonary parenchymal lymphoma at presentation (64,65). Lymphomatous involvement of the pleura manifests most commonly as an infiltrative pleura-based soft-tissue mass that is usually associated with pleural effusion and thickening, which can be focal, diffuse, nodular, or smooth (64). Adenopathy in the EPS is a common associated finding (Fig 27) (64). Malignant lymphoma originating in the bone is rare and can be seen as a lytic bone lesion with or without cortical invasion or extension into the contiguous soft tissues. Thus, this malignancy can invade the extrapleural fat (66). Treatment of lymphoma depends on the histologic subtype determined after biopsy.

Multiple myeloma (MM) is a hematologic malignancy that manifests as an abnormal accumulation of plasma cells in bone marrow. The main radiologic finding of MM is that of multiple osteolytic lesions caused by the production of an osteoclast-stimulating factor by the neoplastic plasmacytic cells. With advanced disease, extramedullary dissemination of MM can occur in the EPS, but this happens very infrequently. Extramedullary dissemination of MM is characterized by the presence of soft-tissue–attenuation nodules or masses (Fig 28) (67). Pleural effusions occur in approximately 6% of patients with myeloma. The cause is multifactorial, and effusions due to pleural myelomatous involvement are rare, occurring in less than 1% of cases. Furthermore, the pleural effusion with MM may be due to other causes unrelated to MM. Rarely, when the pleural effusion is due to MM involvement, it can be the result of infiltration by myeloma cells from adjacent skeletal or parenchymal locations, direct implantation of plasma cells on the pleura, or mediastinal lymph node infiltration with lymphatic obstruction (68).

Neurogenic tumors, including schwannomas and neurofibromas, and chest wall malignancies such as extraosseous Ewing sarcoma (Askin tumor) and malignant fibrous histiocytoma also can involve the EPS (Fig 29) (69–71). Malignant fibrous histiocytomas uncommonly manifest as primary chest wall neoplasms. In this location, the ETF, subcutaneous soft tissue, and skeletal muscle are usually involved (70,71).

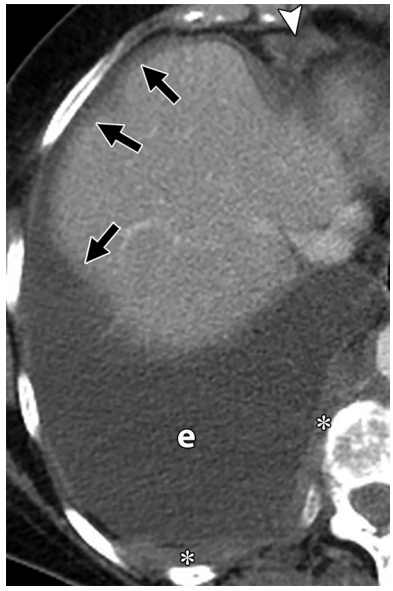

Figure 27. Lymphoma involving the EPS. Axial cropped CT image of the right side of the chest shows tumors in the posterior EPS and paravertebral EPS (*), and retrocrural region. Pleural effusion *(e)* and involvement of the diaphragmatic pleura are seen as subtle pleural thickening (arrows). Right epiphrenic lymphadenopathies (arrowhead) also are seen.

Figure 28. Multiple myeloma. Axial cropped CT image shows a large soft-tissue mass (*) involving the EPS and intercostal plane, multiple tumoral nodules (white arrows) in the EPS, and a mass *(m)* in the right chest wall. Pleural effusion *(e)* and lytic bone lesions (black arrows) in the ribs also are seen.

Miscellaneous Disorders

Extramedullary hematopoiesis arising as a soft-tissue formation in almost any area of the body represents a compensatory state. It occurs when the bone marrow is unable to produce the necessary amount of red blood cells. Extramedullary hematopoiesis can be seen in association with several hematologic diseases, including chronic hemolytic anemia with hemoglobinopathy, and is more frequently seen in patients affected by thallasemia, myelofibrosis, polycythemia vera, leukemia, or lymphoma, or after bone marrow ablation. It typically manifests as a mass or multiple masses, and it develops in the paraspinal EPS (Fig 30) in 11%–15% of cases (72,73).

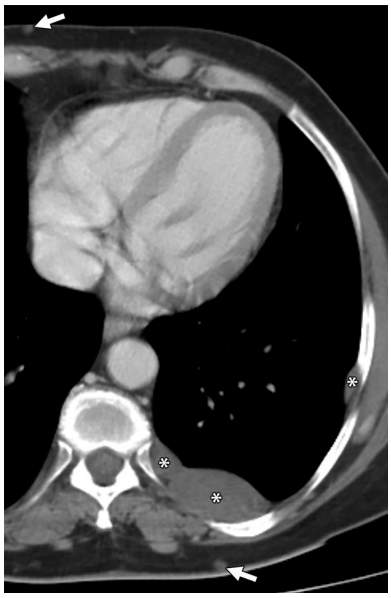

Figure 29. Neurofibromatosis type 1 and neurofibromas in the EPS. Axial cropped CT image shows multiple extrapleural (*) and subcutaneous (arrows) neurofibromas.

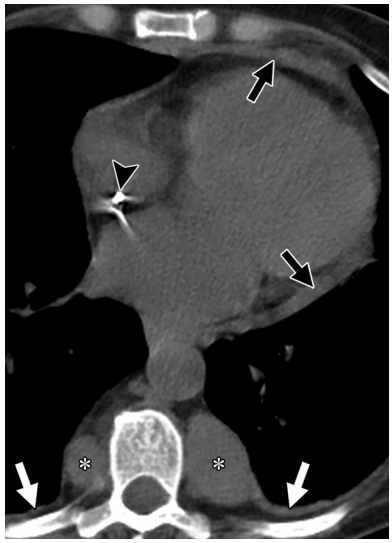

Figure 30. Extramedullary hematopoiesis in the EPS. Axial cropped CT image shows pleural thickening (white arrows), increased linear attenuation and stranding, and masses (*) in the EPS. Note the pacemaker electrode (arrowhead) and small pericardial effusions (black arrows).

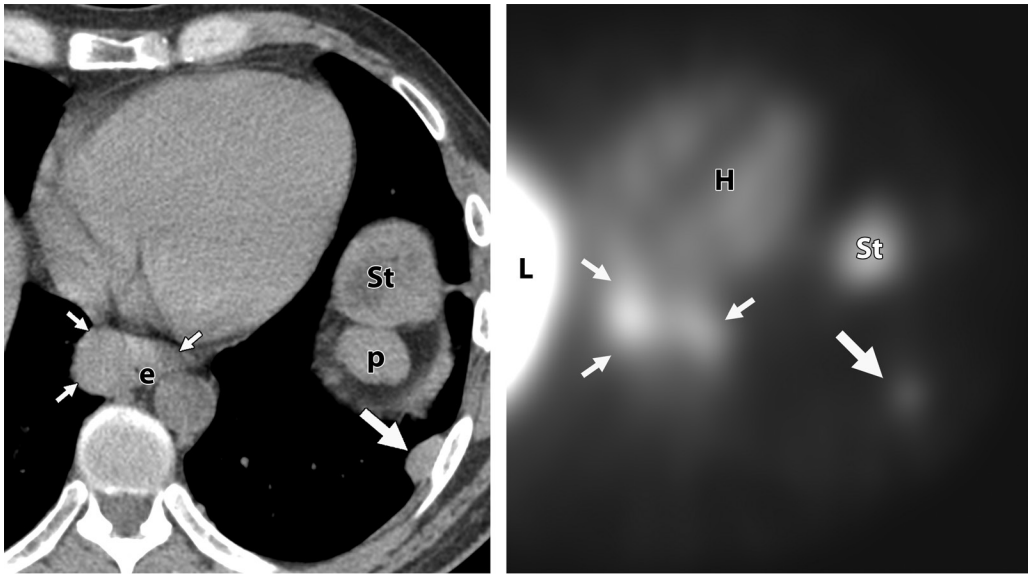

a. **b.**

Figure 31. Thoracic splenosis in a patient with a history of remote severe splenic trauma. Axial cropped **(a)** and ^{99m}Tc–sulfur colloid single photon emission **(b)** CT images show thoracic splenosis (large arrow), manifesting as a soft-tissue–attenuation mass in the EPS, with radioactive tracer uptake. Another mediastinal implant (small arrows) has similar uptake. The left hemidiaphragm is elevated, and the native spleen is absent owing to splenectomy. Intrathoracic sulfur colloid uptake is always an abnormal finding and indicates the presence of ectopic reticuloendothelial tissue, consistent with thoracic splenosis in this case. *e* = esophagus, *H* = heart, *L* = liver, *p* = pancreas tail, *St* = stomach. (Images courtesy of Stefano Rinaldi, MD, Clínica Alemana, Santiago, Chile.)

Splenosis secondary to thoracoabdominal trauma occurs as a result of splenic disruption and autotransplantation of splenic tissue into the pleural cavity, chest wall, or diaphragm. It also manifests as a mass or multiple masses in the EPS, with attenuation and enhancement similar to those of the normal spleen, and should be suspected when lesions are found in the left hemithorax in a patient with a history of abdominal trauma. The diagnosis of thoracic splenosis can be confirmed by using technetium 99m (^{99m}Tc) sulfur colloid scintigraphy or ^{99m}Tc-tagged heat-damaged red blood cells, the latter being more sensitive and specific (44) (Fig 31).

Figure 32. Amyloid deposition in the EPS. Axial cropped CT image shows a mass (*) with punctate calcification in the EPS, and air in the spinal canal due to recent surgery. Note the lytic rib involvement, extension of the soft-tissue mass into the spinal canal, and postsurgical changes of the vertebral body.

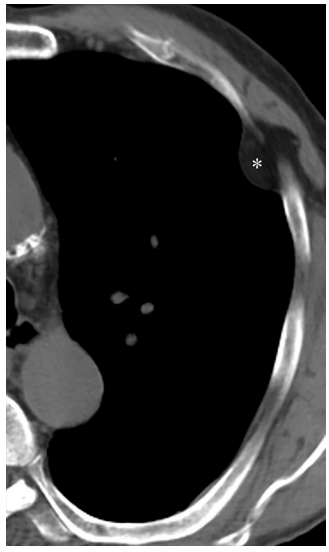

Figure 33. Lipoma mimicking focal thickening of the EPS. Axial cropped CT image shows an intercostal lipoma (*) in the EPS.

Amyloidosis is characterized by the extracellular deposition of immunoglobulin light chains. Although rare, localized pleural amyloidosis can involve the EPS (Fig 32) (74).

Mimicking Pathologic Processes

Various entities can mimic an increase in focal extrapleural adipose tissue. Lipomas are benign encapsulated fatty neoplasms that originate in the EPS (Fig 33) (75). Lipomas mainly cause incidental imaging findings and are rarely symptomatic. Chest wall and diaphragmatic hernias also can mimic increased focal extrapleural adipose tissue (76). Adult Bochdalek hernias, also known as posterior diaphragmatic defects, probably arise as the result of a congenital weakness in the region of the pleuroperitoneal membranes. The incidence of these hernias increases with age and in patients who have chronic obstructive pulmonary disease. They are more frequently found in women, in association with pregnancy and pregnancy-related labor. Posterior diaphragmatic defects are usually located posteriorly in the left hemithorax, and intrathoracic herniation of retroperitoneal adipose tissue can result in a localized increase in extrapleural fat in the EPS (Fig 34) (77).

Conclusion

The EPS is an important anatomic region that is often overlooked at imaging. Chronic inflammation and/or infection, trauma, neoplastic disease, several infiltrative disorders, and splenosis can involve the EPS. Awareness of the normal anatomy of the EPS and recognition of the manifestations of disease arising in or extending into the EPS from the lung, pleura, chest wall, or other thoracic structures, as seen on thin-section CT images, can aid in the diagnosis and evaluation of thoracic diseases and help guide treatment.

References

1. Sugarbaker DJ, Jaklitsch MT, Bueno R, et al. Prevention, early detection, and management of complications after 328 consecutive extrapleural pneumonectomies. J Thorac Cardiovasc Surg 2004;128(1):138–146.
2. Vix VA. Extrapleural costal fat. Radiology 1974;112(3):563–565.
3. Im JG, Webb WR, Rosen A, Gamsu G. Costal pleura: appearances at high-resolution CT. Radiology 1989;171(1):125–131.
4. Hammerman AM, Susman N, Strzembosz A, Kaiser LR. The extrapleural fat sign: CT characteristics. J Comput Assist Tomogr 1990;14(3):345–347.
5. Rahman NM, Wang NS. Anatomy of the pleura. In: Light RW, Lee YCG, eds. Textbook of pleural diseases. 2nd ed. Boca Raton, Fla: CRC, 2008; 13–25.
6. Negrini D, Moriondo A. Pleural function and lymphatics. Acta Physiol (Oxf) 2013;207(2):244–259.
7. Zocchi L. Physiology and pathophysiology of pleural fluid turnover. Eur Respir J 2002;20(6):1545–1558.
8. Wang ZB, Li M, Li JC. Recent advances in the research of lymphatic stomata. Anat Rec (Hoboken) 2010;293(5):754–761.
9. Miura T, Shimada T, Tanaka K, Chujo M, Uchida Y. Lymphatic drainage of carbon particles injected into the pleural cavity of the monkey, as studied by video-assisted thoracoscopy and electron microscopy. J Thorac Cardiovasc Surg 2000;120(3):437–447.
10. Negrini D, Moriondo A. Lymphatic anatomy and biomechanics. J Physiol 2011;589(pt 12):2927–2934.
11. Sharma A, Fidias P, Hayman LA, Loomis SL, Taber KH, Aquino SL. Patterns of lymphadenopathy in thoracic malignancies. RadioGraphics 2004;24(2):419–434.
12. Moore AJ, Parker RJ, Wiggins J. Malignant mesothelioma. Orphanet J Rare Dis 2008;3:34.
13. Benamore RE, Warakaulle DR, Traill ZC. Imaging of pleural disease. Imaging 2008;20(4):236–251.
14. Webb WR, Higgins CB. Thoracic imaging: pulmonary and cardiovascular radiology. 2nd ed. Philadelphia, Pa: Lippincott, Williams & Wilkins, 2011; 623–625.
15. Dewhurst C, O'Neill S, O'Regan K, Maher M. Demonstration of the course of the posterior intercostal artery on CT angiography: relevance to interventional radiology procedures in the chest. Diagn Interv Radiol 2012;18(2):221–224.

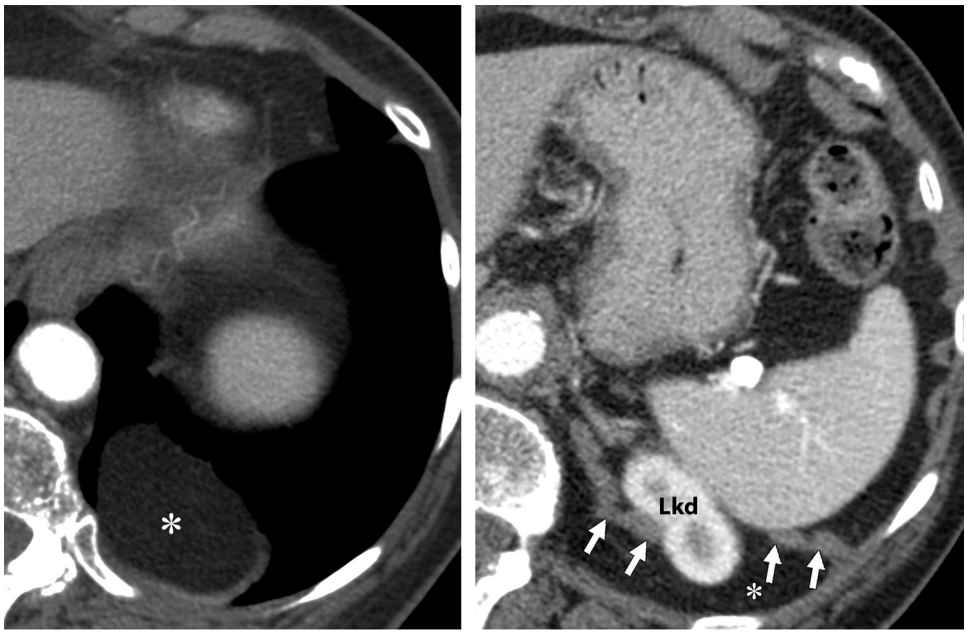

a. b.

Figure 34. Posterior diaphragmatic defect mimicking focal thickening of the EPS. Axial CT images show intrathoracic herniation of retroperitoneal adipose tissue, manifesting as a localized increase in extrapleural fat (*). In **b,** a defect is seen in the posterior aspect of the left hemidiaphragm (arrows) in relation to a slight prominence of the contour of the superior pole of the left kidney *(Lkd),* which is slightly ascended.

16. Pond CM. Adipose tissue and the immune system. Prostaglandins Leukot Essent Fatty Acids 2005;73(1):17–30.
17. Sadler D, Mattacks CA, Pond CM. Changes in adipocytes and dendritic cells in lymph node containing adipose depots during and after many weeks of mild inflammation. J Anat 2005;207(6):769–781.
18. Metintas M, Ucgun I, Elbek O, et al. Computed tomography features in malignant pleural mesothelioma and other commonly seen pleural diseases. Eur J Radiol 2002;41(1):1–9.
19. Waite RJ, Carbonneau RJ, Balikian JP, Umali CB, Pezzella AT, Nash G. Parietal pleural changes in empyema: appearances at CT. Radiology 1990;175(1):145–150.
20. Strange C. Hemothorax. Semin Respir Crit Care Med 1995;16(4):324–332.
21. Batra P, Brown K, Hayashi K, Mori M. Rounded atelectasis. J Thorac Imaging 1996;11(3):187–197.
22. Stathopoulos GT, Karamessini MT, Sotiriadi AE, Pastromas VG. Rounded atelectasis of the lung. Respir Med 2005;99(5):615–623.
23. Peacock C, Copley SJ, Hansell DM. Asbestos-related benign pleural disease. Clin Radiol 2000;55(6):422–432.
24. Woodring JH. Pleural effusion is a cause of round atelectasis of the lung. J Ky Med Assoc 2000;98(12):527–532.
25. Roach HD, Davies GJ, Attanoos R, Crane M, Adams H, Phillips S. Asbestos: when the dust settles—an imaging review of asbestos-related disease. RadioGraphics 2002;22(Spec No):S167–S184.
26. Corcoran JP, Ahmad M, Mukherjee R, Redmond KC. Pleuro-pulmonary complications of rheumatoid arthritis. Respir Care 2014;83(3):324–328.
27. Husain AN, Mirza MK, Gibbs A, et al. How useful is GLUT-1 in differentiating mesothelial hyperplasia and fibrosing pleuritis from epithelioid and sarcomatoid mesotheliomas? an international collaborative study. Lung Cancer 2014;83(3):324–328.
28. Corcoran JP, Ahmad M, Mukherjee R, Redmond KC. Pleuro-pulmonary complications of rheumatoid arthritis. Respir Care 2014;59(4):e55–e59.
29. Takasugi JE, Godwin JD, Teefey SA. The extrapleural fat in empyema: CT appearance. Br J Radiol 1991;64(763):580–583.
30. Kim HY, Song KS, Lee HJ, Lee JS, Lim TH. Parietal pleura and extrapleural space in chronic tuberculous empyema: CT-pathologic correlation. J Comput Assist Tomogr 2001;25(1):9–15.
31. Glicklich M, Mendelson DS, Gendal ES, Teirstein AS. Tuberculous empyema necessitatis: computed tomography findings. Clin Imaging 1990;14(1):23–25.
32. Kuhlman JE, Singha NK. Complex disease of the pleural space: radiographic and CT evaluation. RadioGraphics 1997;17(1):63–79.
33. Kim TS, Han J, Koh WJ, et al. Thoracic actinomycosis: CT features with histopathologic correlation. AJR Am J Roentgenol 2006;186(1):225–231.
34. Ip M, Chen NK, So SY, Chiu SW, Lam WK. Unusual rib destruction in pleuropulmonary tuberculosis. Chest 1989;95(1):242–244.
35. Mehndiratta A, Lawande D, D'costa L. Empyema necessitans following osteomyelitis of rib. Ind J Tuberc 1999;46(1):45–48.
36. Agrawal V, Joshi MK, Jain BK, Mohanty D, Gupta A. Tuberculotic osteomyelitis of rib: a surgical entity. Interact Cardiovasc Thorac Surg 2008;7(6):1028–1030.
37. Mohanty D, Agrawal V, Jain BK, Gupta R, Rathi V, Gupta A. Osteomyelitis of the ribs: a strategy for prompt diagnosis and effective management. Trop Doct 2008;38(4):239–241.
38. Bishara J, Gartman-Israel D, Weinberger M, Maimon S, Tamir G, Pitlik S. Osteomyelitis of the ribs in the antibiotic era. Scand J Infect Dis 2000;32(3):223–227.
39. Singh SK, Gupta V, Ahmad Z, Bhargava R, Pandey DK, Sachdeva S. Tubercular osteomyelitis of rib: case report. Respir Med CME 2009;2(3):128–129.
40. Rashid MA, Wikström T, Ortenwall P. Nomenclature, classification, and signficance of traumatic extrapleural hematoma. J Trauma 2000;49(2):286–290.
41. Chung JH, Carr RB, Stern EJ. Extrapleural hematomas: imaging appearance, classification, and clinical significance. J Thorac Imaging 2011;26(3):218–223.
42. Sumida H, Ono N, Terada Y. Huge extrapleural hematoma in an anticoagulated patient. Gen Thorac Cardiovasc Surg 2007;55(4):174–176.

43. Igai H, Okumura N, Ohata K, Matsuoka T, Kameyama K, Nakagawa T. Rapidly expanding extrapleural hematoma. Gen Thorac Cardiovasc Surg 2008;56(10):515–517.
44. Walker CM, Takasugi JE, Chung JH, et al. Tumorlike conditions of the pleura. RadioGraphics 2012;32(4):971–985.
45. Chen JM, Lv J, Ma K, Yan J. Assessment of internal mammary artery injury after blunt chest trauma: a literature review. J Zhejiang Univ Sci B 2014;15(10):864–869.
46. Rozeik C, Kotterer O, Deiningr HK. Pneumothorax simulated by detachment of parietal pleura associated with pneumomediastinum. Eur Radiol 1994;4(5):496–499.
47. Zylak CM, Standen JR, Barnes GR, Zylak CJ. Pneumomediastinum revisited. RadioGraphics 2000;20(4):1043–1057.
48. Kurihara Y, Nakajima Y, Niimi H, Arakawa H, Ishikawa T. Extrapleural air collections mimicking pneumothorax: helical CT finding. J Comput Assist Tomogr 1997;21(5):771–772.
49. Lillard RL, Allen RP. The extrapleural air sign in pneumomediastinum. Radiology 1965;85(6):1093–1098.
50. Kim SE, Lee SH, Lee CJ, et al. Extrapleural fat hypertrophy in patients with lung cancer: CT findings [in Korean]. J Korean Radiol Soc 1994;31(4):673–678.
51. Kozower BD, Larner JM, Detterbeck FC, Jones DR. Special treatment issues in non-small cell lung cancer: diagnosis and management of lung cancer, 3rd ed—American College of Chest Physicians evidence-based clinical practice guidelines. Chest 2014;143(5 suppl):e369S–e399S.
52. Matsuoka H, Nishio W, Okada M, Sakamoto T, Yoshimura M, Tsubota N. Resection of chest wall invasion in patients with non-small cell lung cancer. Eur J Cardiothorac Surg 2004;26(6):1200–1204.
53. Deslauriers J, Tronc F, Fortin D. Management of tumors involving the chest wall including pancoast tumors and tumors invading the spine. Thorac Surg Clin 2013;23(3):313–325.
54. Qi LP, Li XT, Yang Y, et al. Multivariate analysis of pleural invasion of peripheral non-small cell lung cancer-based computed tomography features. J Comput Assist Tomogr 2016;40(5):757–762.
55. Ratto GB, Piacenza G, Frola C, et al. Chest wall involvement by lung cancer: computed tomographic detection and results of operation. Ann Thorac Surg 1991;51(2):182–188.
56. Akata S, Kajiwara N, Park J, et al. Evaluation of chest wall invasion by lung cancer using respiratory dynamic MRI. J Med Imaging Radiat Oncol 2008;52(1):36–39.
57. Caroli G, Dell'Amore A, Cassanelli N, et al. Accuracy of transthoracic ultrasound for the prediction of chest wall infiltration by lung cancer and of lung infiltration by chest wall tumours. Heart Lung Circ 2015;24(10):1020–1026.
58. Rusch VW, Giroux D, Kennedy C, et al. Initial analysis of the international association for the study of lung cancer mesothelioma database. J Thorac Oncol 2012;7(11):1631–1639.
59. Rice DC, Stevens CW, Correa AM, et al. Outcomes after extrapleural pneumonectomy and intensity-modulated radiation therapy for malignant pleural mesothelioma. Ann Thorac Surg 2007;84(5):1685–1692; discussion 1692–1693.
60. Kent M, Rice D, Flores R. Diagnosis, staging, and surgical treatment of malignant pleural mesothelioma. Curr Treat Options Oncol 2008;9(2-3):158–170.
61. Goldstraw P, Crowley J, Chansky K, et al. The IASLC Lung Cancer Staging Project: proposals for the revision of the TNM stage groupings in the forthcoming (seventh) edition of the TNM classification of malignant tumours. J Thorac Oncol 2007;2(8):706–714.
62. Ai J, Stevenson JP. Current issues in malignant pleural mesothelioma evaluation and management. Oncologist 2014;19(9):975–984.
63. Wolf AS, Flores RM. Current treatment of mesothelioma: extrapleural pneumonectomy versus pleurectomy/decortication. Thorac Surg Clin 2016;26(3):359–375.
64. Aquino SL, Chen MY, Kuo WT, Chiles C. The CT appearance of pleural and extrapleural disease in lymphoma. Clin Radiol 1999;54(10):647–650.
65. Shuman LS, Libshitz HI. Solid pleural manifestations of lymphoma. AJR Am J Roentgenol 1984;142(2):269–273.
66. Nishiyama N, Nakatani S, Inoue K, Katoh T, Kinoshita H. Primary lymphoma of bone originating in a rib. Jpn J Thorac Cardiovasc Surg 2000;48(3):180–183.
67. Kushwaha RA, Verma SK, Mehra S, Prasad R. Pulmonary and nodal multiple myeloma with a pleural effusion mimicking bronchogenic carcinoma. J Cancer Res Ther 2009;5(4):297–299.
68. Alexandrakis MG, Passam FH, Kyriakou DS, Bouros D. Pleural effusions in hematologic malignancies. Chest 2004;125(4):1546–1555.
69. Restrepo CS, Herrera DA, Lemos JA. Extraforaminal meningioma with extrapleural space extension. AJR Am J Roentgenol 2006;186(5):1314–1316.
70. Dou X, Yan H, Wang R. Treatment of an Askin tumor: a case report and review of the literature. Oncol Lett 2013;6(4):985–989.
71. Liu Y, Chen G, Wu Y, et al. Combined pulmonary lobectomy for surgical treatment of a malignant fibrous histiocytoma of the chest wall: a case report. Diagn Pathol 2014;9:21.
72. Boiselle PM, Rosado-de-Christenson ML. Fat attenuation lesions of the mediastinum. J Comput Assist Tomogr 2001;25(6):881–889.
73. Haidar R, Mhaidli H, Taher AT. Paraspinal extramedullary hematopoiesis in patients with thalassemia intermedia. Eur Spine J 2010;19(6):871–878.
74. Yoshiya S, Maruyam a R, Koga T, Shikada Y, Yano T, Maehara Y. Localized pleural amyloidosis: report of a case. Surg Today 2012;42(6):597–600.
75. Gaerte SC, Meyer CA, Winer-Muram HT, Tarver RD, Conces DJ Jr. Fat-containing lesions of the chest. RadioGraphics 2002;22(Spec No):S61–S78.
76. Fisher ER, Godwin JD. Extrapleural fat collections: pseudotumors and other confusing manifestations. AJR Am J Roentgenol 1993;161(1):47–52.
77. Caskey CI, Zerhouni EA, Fishman EK, Rahmouni AD. Aging of the diaphragm: a CT study. Radiology 1989;171(2):385–389.